Onset and dynamics of avalanches in a rotating cylinder: From experimental data to a geometric model

Christopher P. McLaren,[1] Bernhard J. Leistner,[1] Sebastian Pinzello,[1] Eduardo Cano-Pleite,[2] and Christoph R. Müller[1,*]
[1]*Department of Mechanical and Process Engineering, ETH Zurich, Leonhardstrasse 21, 8092 Zurich, Switzerland*
[2]*Thermal and Fluids Engineering Department, Carlos III University of Madrid, Avda. de la Universidad 30, 28911 Leganés, Spain*

(Received 1 December 2021; accepted 9 September 2022; published 15 November 2022)

Particle image velocimetry has been applied to measure particle velocities on the free surface of a bed of particles within a rotating cylinder during avalanching. The particle velocities were used to examine the validity of existing avalanche models and to propose an alternative model. The movement of particles depends on their location on the surface of the bed: Particles located near the center of the bed travel the farthest, while the distance traveled decreases at an increasing rate for particles located farther from the center. The start of an avalanche can be determined to a single initiation point that can be located on the bottom half of the bed; the avalanche quickly propagates through the entire free surface with 90% of the surface in motion within 257 ms (approximately 20% of the total duration of an avalanche). The experimental insight is used to formulate a geometric model, in which three equal-sized sections flow down the bed surface during an avalanch. The predictions of the model are validated by experimental mixing measurements.

DOI: 10.1103/PhysRevE.106.054902

I. INTRODUCTION

Rotating drums are key for the processing of materials in the mineral, ceramic, metallurgical, chemical, pharmaceutical, waste, and food industries [1–14]. A rotating cylinder can operate in different regimes. Among them, the avalanching regime is a quasiperiodic motion that is observed at low rotation speeds. In the avalanching regime the bed rotates as a rigid body until a section of the bed breaks off and moves down the free surface as an avalanche. The avalanche reduces the angle that the free surface of the bed forms with the horizontal. Figure 1 visualizes a simple geometric model of the bed surface before an avalanche (angle θ_s) and after an avalanche (angle θ_t). Following an avalanche, the bed returns to rigid-body rotation and the angle between the bed's free surface and the horizontal increases until the next avalanche is initiated. Following the work of Bak *et al.* [15] of self-organized criticality, avalanching within rotating cylinders has received considerable attention [16–18].

Today there exist multiple competing models for the avalanching regime [19]. Metcalfe *et al.* [20] presented a model for particle mixing in the avalanche regime and compared predictions from their model with results from experiments performed in a pseudo–two-dimensional rotating cylinder. The basis of their model was a geometric argument that the result of an avalanche event is to transport a wedge of material from the top half of the surface (blue in Fig. 1) down the free surface such that after the avalanche it occupies a new wedge at the bottom half of the free surface (green in Fig. 1). The lines defining these wedges are the free surfaces of the bed before and after the avalanche has occurred, and it was assumed that no particles outside of this wedge are affected by the avalanche. Based on this model it was argued that the problem of mixing within a system operating in the avalanching regime may be decomposed into two parts: the transport of wedges and mixing within wedges. In the absence of more detailed information, random mixing within the wedges was assumed. This wedge model was refined further by McCarthy *et al.* [21].

Lim *et al.* [22] performed positron emission particle tracking (PEPT) studies of sand rotated in a horizontal cylinder that was operated in the avalanching regime. The PEPT data revealed that on average, a particle on the free surface was involved in more than one avalanche before it rejoined the bulk of the bed in rigid-body rotation. The average number of avalanches required for a particle to traverse the free surface was found to depend on the rotational Froude number ($\mathrm{Fr} = \omega^2 R/g$), where ω is the rotational speed, R is the radius of the cylinder, and g is the gravitational acceleration. At low values of Fr, particles remained on the free surface for an average of 4.25 avalanches, whereas this number dropped to 1 avalanche when the bed was operated in the rolling regime with $\mathrm{Fr} = 1.47 \times 10^{-4}$. They found the average number of avalanches required for a particle to traverse the free surface to linearly decrease with increasing Fr.

These observations do not support the geometric wedge model of avalanches proposed by Metcalfe *et al.* [20] since the geometric model implies that particles traverse the free surface in a single avalanche. In light of their observations, Lim *et al.* [22] proposed a modified wedge model in which the centroid of the avalanching material moves a distance 1/3 of the chord length (L) down the free surface (see Fig. 1).

So far, studies that have investigated mixing in the avalanching regime in rotating cylinders have not tracked the overall motion of all particles. Lim *et al.* [22] tracked only

*muelchri@ethz.ch

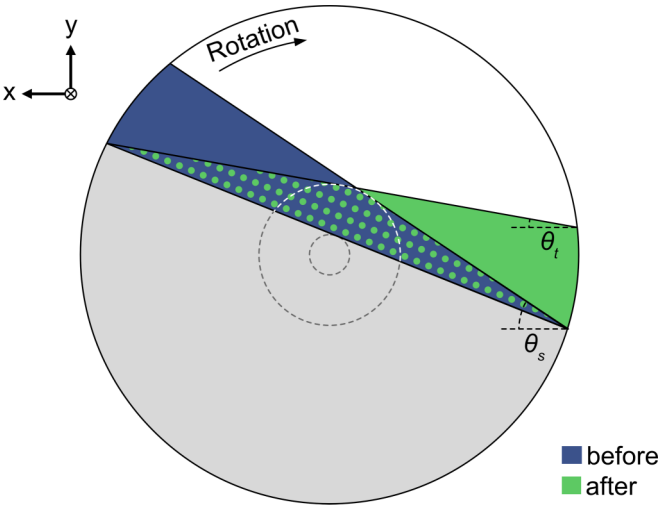

FIG. 1. Geometric avalanche models where θ_s is the angle between the bed surface and the horizontal before an avalanche and θ_t is the corresponding angle after an avalanche event: the model proposed by Metcalfe *et al.* [20] has the purely blue wedge becoming the purely green wedge after an avalanche event. The model proposed by Lim *et al.* [22] has the wedge made of all areas containing blue color become the wedge of all areas containing green color.

a single particle using PEPT. Courrech du Pont *et al.* [23] tracked the flowing surface averaging the velocities along the surface flow. Kiesgen de Richter *et al.* [24] studied grain rearrangements by using a camera and observed the acoustic amplitude across the bed using a piezotransducer and receiver, allowing them to observe changes in the weak contacts, i.e., contact forces lower than the designated cutoff force. In addition, Kiesgen de Richter *et al.* [24], Gravish and Goldman [25], and Zaitsev *et al.* [26] observed precursors to avalanches whereby small changes in the packing lead to small rearrangements of the free surface, but surface flow did not occur. Furthermore, Zaitsev *et al.* [26] observed a slow relaxation of particle displacements to an equilibrium position after the avalanche.

In order to examine the validity of the geometric models proposed by Metcalfe *et al.* [20] and Lim *et al.* [22], particle image velocimetry (PIV) is applied in this work to investigate the motion of the particles on the bed surface during avalanches in a rotating cylinder. Utilizing our experimental findings, an alternative geometric model for mixing during avalanching is proposed and compared against experimental measurements.

Concerning the modeling of avalanches, discrete element modeling (DEM) of avalanching has been reported with a focus on investigating the initiation mechanism of avalanches [27–29]. The modeling of the full avalanching process remains difficult due to the inherent hysteresis of granular material (e.g., angle of repose) when switching between static and flowing states [30]. Indeed, recent modeling works on avalanching caution that the results obtained are qualitative rather than quantitative [31]. DEM simulations also require a large set of predetermined particle properties such as the elastic modulus and Poisson's ratio, and particle interaction properties such as the coefficients of restitution and friction.

TABLE I. Drums.

	Drum 1	Drum 2	Drum 3
Inner diameter D (mm)	94	140	290
Length (mm)	400	400	400

On the other hand, the geometric model reported here provides a simple, yet realistic description of mixing during avalanching.

II. EXPERIMENT SETUP

In this work three drums of different diameters (see Table I) were studied. The drums were constructed out of clear Polymethylmethacrylat with walls of thickness 5 mm, allowing two cameras an unobstructed view to the top surface and the side of the drums. Drum 2 was filled with particles to fill levels ranging from 20 to 70% with 5% increments. Three differently sized spherical particles, as shown in Table II, were studied. In order to perform PIV, 10% of the particles were darker colored (but otherwise identical) to allow PIV. The light-colored particles were purchased clear but quickly become opaque with usage. When first used the clear particles severely hindered the view on the black particles below the very top layer and with usage it became completely impossible to see through them. Therefore, we considered to have filmed the top layer only. The cylinder was driven by a motor (Maxon EPOS 2 24/5) and the free surface of the bed was imaged using a high-speed camera (Nikon, 496RC2) with a frame rate of 100 frames per second and a resolution of 1280 × 1024 pixels for PIV purposes. A Canon EOS camera filmed the side of the drum to determine the slope of the free surface of the bed. In order to avoid possible effects due to visual distortion by the Plexiglas walls, the top 5% of the free surface was discounted for the determination of the distances traveled by the particles. The bottom 10% was discounted due to particles overtaking each other, as explained later in the paper.

The particle velocities were calculated using the MATPIV 1.6.1 software [32]. The size of the PIV interrogation window was iteratively reduced from 64 × 64 to 32 × 32 pixels, using four iterations. Once the velocities were determined, a signal-to-noise filter (S/N = 1.3), and global and local mean filters were applied to detect outliers [33]. To ensure a statistical significance of the results, 14–20 avalanches were averaged.

III. RESULTS

Figure 2 shows the time evolution of the slope of the free surface of the bed for drum diameters of 94, 140, and 290 mm. For all drum diameters the evolution of the slope of the free

TABLE II. Spherical particles.

	Ballotini 1	Ballotini 2	Ballotini 3
Diameter d (mm)	1.0–1.3	2.0–2.4	2.85–3.45
Material	Glass	Glass	Glass
Density (kg/dm^3)	2.5	2.5	2.5

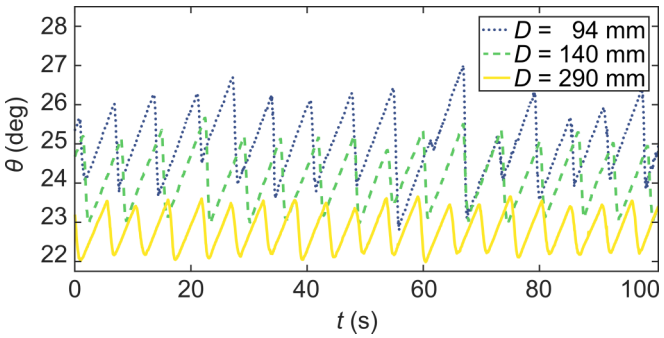

FIG. 2. Slope of the free surface (θ) as a function of time (t) for three drum diameters: 94 mm (dotted blue), 140 mm (dashed green), and 290 mm (yellow) rotating at 0.066 rpm and a fill level of 25%. The particles have a diameter of 1.0–1.3 mm.

surface shows a "sawtooth" pattern that is characteristic of the avalanching regime; individual avalanches can be identified as a rapid decrease in the slope of the free surface and between avalanches the slope increases linearly with time, indicating rigid-body rotation.

It can be observed that avalanching is a quasiperiodic phenomenon with fluctuations in both the magnitude of the slope change during an avalanche and the time between successive avalanches. In agreement with Daerr and Douady [34], the avalanches appear to become more regular as the drum diameter is increased, i.e., increasing the Froude number. The change in surface angle over an avalanche event increases with decreasing drum size, i.e., rising from 1.5° for $D =$ 290 mm to 2.1° for $D = 94$ mm. This is consistent with the work of Balmforth and McElwaine [35], who showed that as d/D increases so does the change in surface angle during an avalanche event.

In the following, the particle motion at the start of an avalanche will be considered. In this work, the start of motion was defined as the moment when an interrogation window of particles exceeded the threshold velocity $v_t = 3\,\mathrm{mm/s}$. This threshold velocity was found to have a negligible impact on the results when set between 1 and 20 mm/s (*vide infra*). Rearrangements on the surface, described in previous studies [24] as precursors to an avalanching event were observed but no interrogation window exceeded the avalanching threshold velocity of 3 mm/s.

The avalanche's initiation time was found to be insensitive to this velocity threshold. When varying the threshold between 1 and 20 mm/s, the initiation time is delayed at most by 20 ms, which is less than 2% of the duration of an avalanche (T_{aval}). Furthermore, the location of the initiation point of the avalanche was unaffected by the variation of the velocity threshold and the propagation of the avalanche at the free surface proceeds at the same rate for threshold velocities between 1 and 20 mm/s. Figures 3(a) and 3(b) show the time (t) after the initiation of an avalanche. Figure 3(c) shows the initiation points of avalanches, i.e., the first location to exceed v_t. Data are shown for avalanches in a drum of diameter 140 mm, a particle size range of 1.0–1.3 mm, and a fill level of 25%.

Both Pohlman *et al.* [35] and Rabaud *et al.* [36] showed that the endcaps of the cylinder affect the surface velocity.

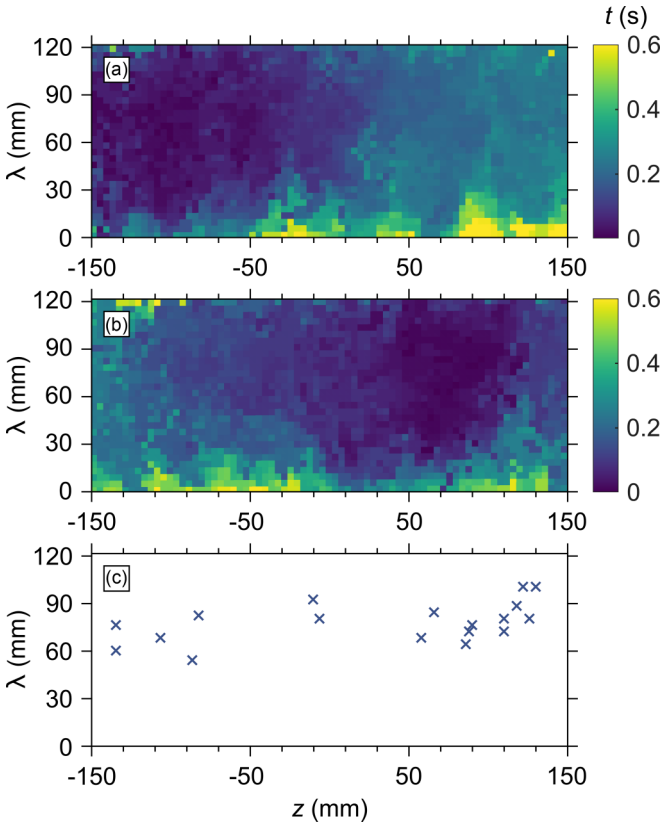

FIG. 3. Local avalanche initiation time (t) shown for two independent avalanche events (a), (b) and a plot of the locations of avalanche initiations (c). In (a) and (b) the color indicates the time after the start of the avalanche for which the velocity at a point on the free surface exceeds 3 mm/s. In (c) the "×" indicates the locations of avalanche initiations for 18 individual avalanches. The cylinder has an internal diameter of 140 mm and rotates at 0.066 rpm. The fill level was 25% and the particles had a diameter in the range 1.0–1.3 mm.

Therefore, a subregion in the center of the cylinder with a width of 300 mm is examined in the PIV experiments such that a representative behavior of the avalanching dynamics, unaffected by the endcaps, is presented.

We observe that an avalanche can be initiated at a variety of locations on the free surface, as was also observed experimentally by Balmforth and McElwaine [37]. It can be seen in Fig. 3(c) that avalanches are initiated at random locations in the axial direction but concentrated in $0.5 < \lambda/L < 0.75$, where λ denotes the position along the chord of the free surface, starting from the bottom. The lowest observed point of initiation is at $\lambda/L = 0.43$, the highest is at $\lambda/L = 0.84$, and the mean is at $\lambda/L = 0.64$ with a standard deviation of ± 0.13.

Figure 4 shows the fraction of the free surface (η) that is involved during an avalanche event as a function of the fraction of the duration of an avalanche event. The fraction of the surface in motion increases linearly for roughly the initial 10% of the duration of the avalanche; subsequently, η increases at a significantly slower rate. On average 90% of the free surface exceeds v_t within 257 ± 98 ms of the start of the avalanche. The average duration of an avalanche is 1.5 s;

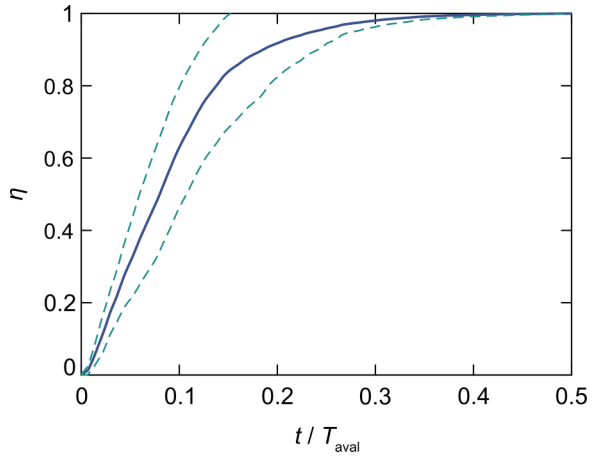

FIG. 4. Fraction of the bed surface involved during an avalanching event (η) as a function of the fraction of the duration of an avalanche event (t/T_{aval}). The mean (solid line) and standard deviation (dashed lines) were calculated from the data of 20 avalanches. The cylinder has a diameter of 140 mm and rotates at 0.066 rpm. The fill level is 25% and the particles are glass ballotini with a diameter of 1.0–1.3 mm.

thus, roughly 1/5 of the avalanche duration is required to bring almost the entire bed surface in motion.

Figure 5 shows the velocities of the avalanching particles at the start of an avalanche, during an avalanche, and at the end of an avalanche. Data are shown for an avalanche with a drum diameter of 140 mm, a particle diameter in the range 1.0–1.3 mm, and a fill level of 25%. At the start of the avalanche, only a concentrated area of particles around the location of the initiation point of the avalanche shows some motion while the rest of the surface does not show any relative motion. The maximal speed averaged across the bed surface (54 mm/s) was attained 0.59 s after the start of the avalanche. At this point, the entire bed is in motion and appears to move uniformly down the slope as shown in Fig. 5(b). In contrast to the beginning of the avalanche, where the trigger of the avalanche could be traced to an individual starting point, the end of the avalanche has a slow, random relaxation of particle displacements to an equilibrium as observed by Zaitsev *et al.* [26] and Deboeuf *et al.* [38].

The high temporal and spatial resolutions of the PIV measurements reported here allow to estimate the trajectories of particles during an avalanche by integrating the PIV data. Note that PIV calculates the displacement of patterns, rather than of individual particles, with the result that the trajectories obtained in this manner do not represent the exact paths of individual particles. Here, the term "pseudoparticle" will be used to denote a pattern whose trajectory has been calculated by integrating PIV data. Pseudoparticles were initialized at the center of the PIV interrogation windows, and their velocities were tracked for the duration of the avalanche.

Figure 6 shows the distances traveled down the chord ($\Delta\lambda$) by pseudoparticles during an avalanche as a function of the starting position of the pseudoparticle. The axial displacement during an avalanche event was found to be on average only 2% of the total distance traveled and therefore only the displacement along the free surface is considered for the calculation

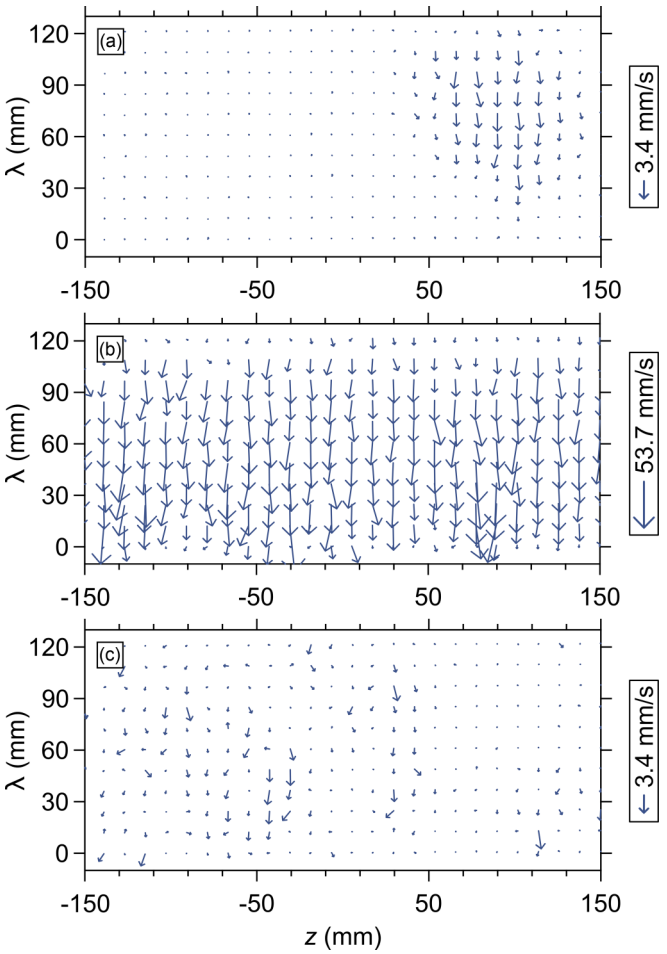

FIG. 5. Velocity of particles at the bed surface during an avalanching event: (a) at the start, (b) at the maximal speed, and (c) at the end of an avalanche, based on PIV calculations. The beginning of an avalanche is defined as the point in time when the first particles exceeded a velocity of 3 mm/s. Maximal speed attained by the avalanching material in the avalanche shown was 54 mm/s. The end of the avalanche was defined as the point when the speed of all pseudoparticles was below 3 mm/s. The cylinder has an internal diameter of 140 mm and rotates at 0.066 rpm. The fill level was approximately 25% and the particles had a diameter of 1.0–1.3 mm.

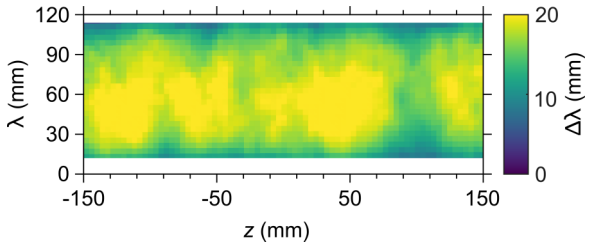

FIG. 6. Distance traveled down the chord by pseudoparticles ($\Delta\lambda$) as a function of their starting positions (λ, z) for an avalanche occurring in a drum of diameter 140 mm. The particles had a diameter of 1.0–1.3 mm. The drum rotated at 0.066 rpm and was filled to a fill level of 25%. The top 5% and bottom 10% of the free surface have been removed to avoid, respectively, the possible effect of visual distortion due to the Polymethylmethacrylat walls at the top of the free surface and particles being overtaken at the bottom of the free surface.

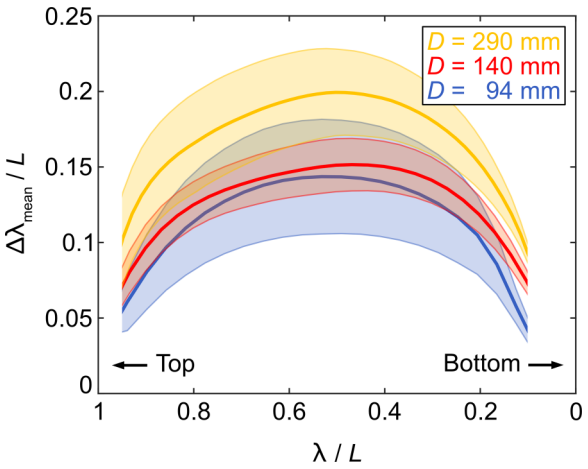

FIG. 7. Mean fraction of the chord length traveled down the chord ($\Delta\lambda_{\text{mean}}/L$) during a single avalanching event as a function of the starting position along the chord (λ/L) for different drum diameters. The data have been averaged over 16 avalanches for each drum diameter. The cylinder had a diameter of either 94 mm (blue line), 140 mm (red line), or 290 mm (yellow line). The correspondingly color-shaded areas represent one standard deviation The fill level was 25% and the particles had a diameter of 1.0–1.3 mm. The drum rotated at 0.066 rpm.

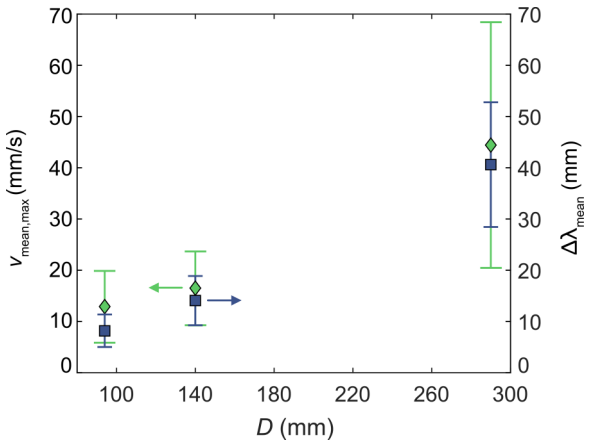

FIG. 8. Maxima of the mean speed ($v_{\text{mean, max}}$) of the entire bed surface (green) and the average distance traveled down the chord ($\Delta\lambda_{\text{mean}}$) (blue) averaged over the entire surface as a function of the drum diameter (D). The error bars represent one standard deviation. The drums rotated at 0.066 rpm. The particles used had a diameter of 1.0–1.3 mm and a fill level of 25%. The lowest 10% of the chord was not accounted for to calculate the distance traveled, as particles located in this part of the chord may have been overtaken by particles initially located higher up the chord.

of the distances traveled. Data are shown for an avalanche in a drum of diameter 140 mm and fill level of 25%. The particles are glass ballotini with a diameter of 1.0–1.3 mm.

The distances traveled for particles located in the lowest 10% of the chord are not shown as they could have been overtaken by particles starting higher up the free surface of the bed. The top 5% of the bed is also not shown to avoid the effect of visual distortion from the Polymethylmethacrylat walls. PIV is only able to track the velocities of particles that remain on the surface. Thus, when a pseudoparticle is overtaken by material flowing over, it is no longer trackable. Any subsequent velocity for this pseudoparticle would correspond to the pseudoparticle that had overtaken it. To avoid using the velocities of a particle that has overtaken the original particle, a control was set in place. In this work a pseudoparticle was assumed to have been overtaken if a particle that started higher up the surface of the bed approached to a distance of less than half an interrogation window. It was found that only pseudoparticles in the lowest 10% of the chord could be overtaken.

Figure 7 plots the average distances traveled by pseudoparticles down the free surface during an avalanche (average of 16 avalanche events) for three different drum diameters. As in Fig. 6 the distance traveled by particles starting in the top 5% and the lowest 10% of the chord are not shown.

The particles located in the center of the bed surface travel the furthest distance, i.e., on average 20% of the chord length for the largest drum diameter (290 mm), whereby the distance traveled decreases with decreasing drum diameter. This is expected as the Froude number decreases with decreasing drum diameter [22].

It can be seen in Fig. 7 that the distance traveled by pseudoparticles decreases at an increasing rate with the distance they are initially located from the center of the chord independent of the drum diameter. This observation can be also made when varying the particle diameter and the fill height, as shown, respectively, in Supplemental Material (SM) Fig. 1 and SM Fig. 2 [39]. Due to the low Froude number, particles travel less than $L/3$ as hypothesized in the model of Lim *et al.* [22]. For $\lambda/L > 0.85$, there is a dramatic decrease in the distance traveled, with the top 5% of the bed surface traveling only 10% of the chord length. Generally, the average distance traveled by an avalanching particle (absolute value) correlated with the chord length of the free surface, i.e., the longest average distance traveled was observed for a fill level of 50%. However, when the distance traveled was normalized by the chord length, the normalized distance traveled was largely independent of the fill level as seen in Fig. SM 3 [39]. The fraction of the chord length traveled as a function of the starting position is typically largest at the center of the chord with the distances traveled decreasing at an increasing rate farther from the center.

The maxima of the average velocity of pseudoparticles are found by determining the velocity between two consecutive frames for all the PIV interrogation windows and averaging those velocities to calculate an instantaneous average velocity of the bed surface. Subsequently, the maximum of the average velocity of the entire free surface during an avalanche is determined for each avalanching event, which is then averaged for an entire series of avalanches and is plotted in Fig. 8 as a function of D. In addition, for each avalanching event the average distance traveled by all pseudoparticles on the entire free surface of the imaged subregion is calculated. Subsequently, these distances are averaged over a series of avalanches. All error bars in Fig. 8 represent one standard deviation. Figure 8 shows clearly that both the maxima of the mean velocity of the particles at the bed surface and the average distance traveled down the chord increased with increasing drum diameter. These findings are consistent with the data plotted in

Fig. 7, i.e., the mean distance traveled during an avalanching event increases with increasing chord length and hence also with increasing drum diameter. This can be explained that with an increasing chord length (i.e., with increasing drum diameter) there is an increasing particle pressure on particles located further down, leading in turn to higher mean particle velocities. In general, a higher average velocity of the particles at the bed surface is expected with increasing Froude number, i.e., with increasing drum diameter.

IV. DISCUSSION

The distance traveled by pseudoparticles along the free surface of the bed depends on their starting location. As seen in Fig. 7, the particles that start in the center of the chord of the free surface travel the farthest and the distance traveled by pseudoparticles decreases at an increasing rate with the distance they are initially located from the center of the chord. This behavior can be understood based on the work by Daerr and Douady [34], which showed that the movement of particles in an avalanche is driven by two effects: the loss of support as the lower-lying particles slide away, and an increase in pressure due to the downward motion of particles that were initially located higher up. At the highest point of the free surface the pressure due to the weight of the particles above is minimal, while at the lowest point of the free surface the motion of particles is hindered by the cylinder wall. On the other hand, at the center of the free surface both effects occur, leading in turn to high avalanche velocities [Fig. 5(b)].

Metcalfe *et al.* [20] proposed a geometric model for avalanches in which it was assumed that an avalanche transports a "wedge" of material from the upper half of the free surface to the lower half of the free surface, as shown in Fig. 1. In this model the lower half of the free surface is not involved in the avalanche and is simply covered by material flowing from the upper half of the free surface. The data presented here are not consistent with this simple geometric model. Figures 3 and 5 clearly demonstrate that avalanches are being initiated in the center of the free surface. The avalanche is then propagated through the surface of the bed, setting its entire surface in motion (Fig. 5), including the lower half of the bed.

Lim *et al.* [22] proposed a modified wedge model. The model of Lim *et al.* [22] assumes that the avalanching material moves an average distance of 1/3 of the chord down the free surface, rather than traveling the entire free surface in one avalanche. Their defined wedge is made up of two chords: the top surface of the bed before and after the avalanche. In accordance with Lim *et al.* [22], who suggested that the number of avalanches required for a particle to traverse the free surface decreases linearly with increasing Fr, we found the average distance traveled by particles in one avalanche to increase with increasing drum diameter.

Although it is possible to fit a linear relationship between the drum diameter and the average distance traveled (as would be expected according to the relationship proposed by Lim *et al.* [22]), a nonlinear relationship is more likely, yet we do not have a sufficient number of experimental data to draw a robust conclusion.

Due to the shape of the wedge in Lim *et al.*'s [22] model, which is shown schematically in Fig. 1, most of the material

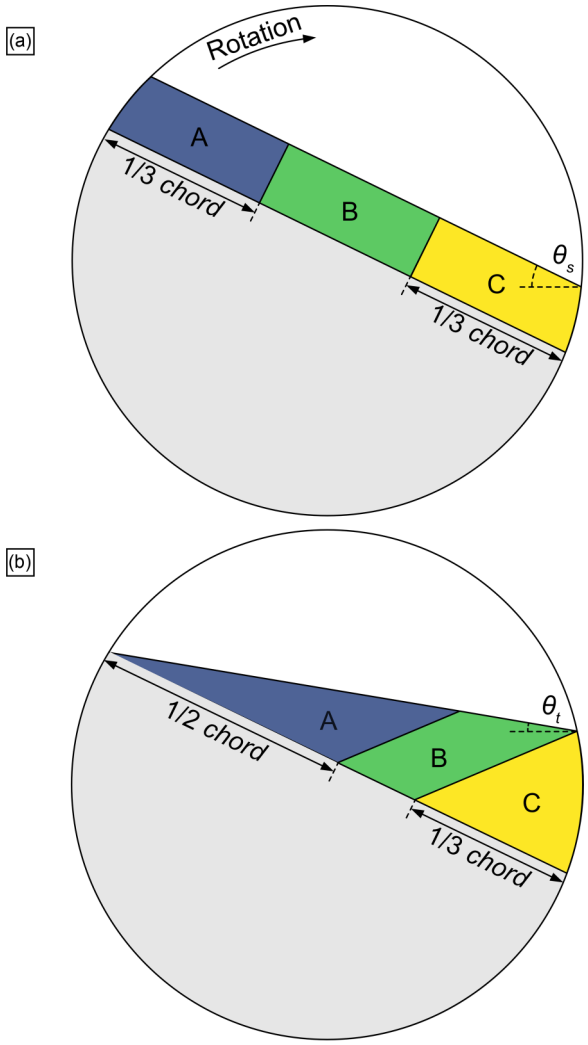

FIG. 9. The geometric avalanche model proposed here based on the experimental PIV data aquired. The flowing layer of the bed is separated into sections A, B, and C: (a) The flowing (avalanching) layer before the avalanching event; (b) Deformation of the initial segments during the avalanching event considering that particles located in the center of the bed move the farthest during an avalanching event.

which flows to the lower wedge is initially located at the top of the free surface. However, in our experiments we observe that particles located at the very top of the bed move significantly less during an avalanche than those in the center of the free surface. Therefore, although the data reported here suggest the model proposed by Lim *et al.* [22] is unlikely, we cannot disprove this model based on our data alone.

Instead, based on our experimental results, showing that particles located in the center of the chord move furthest (Fig. 7), we propose a geometric avalanche model. When creating a geometric model, a trade-off between accuracy and simplicity has to be made. Hence, the model has two objectives: (i) maintain a simple geometry, as has been done in the previous models of Metcalfe *et al.* [20] and Lim *et al.* [22], and (ii) improve the accuracy by taking into account the PIV results which show that the particles in the center of the free surface move the furthest. The proposed model is sketched

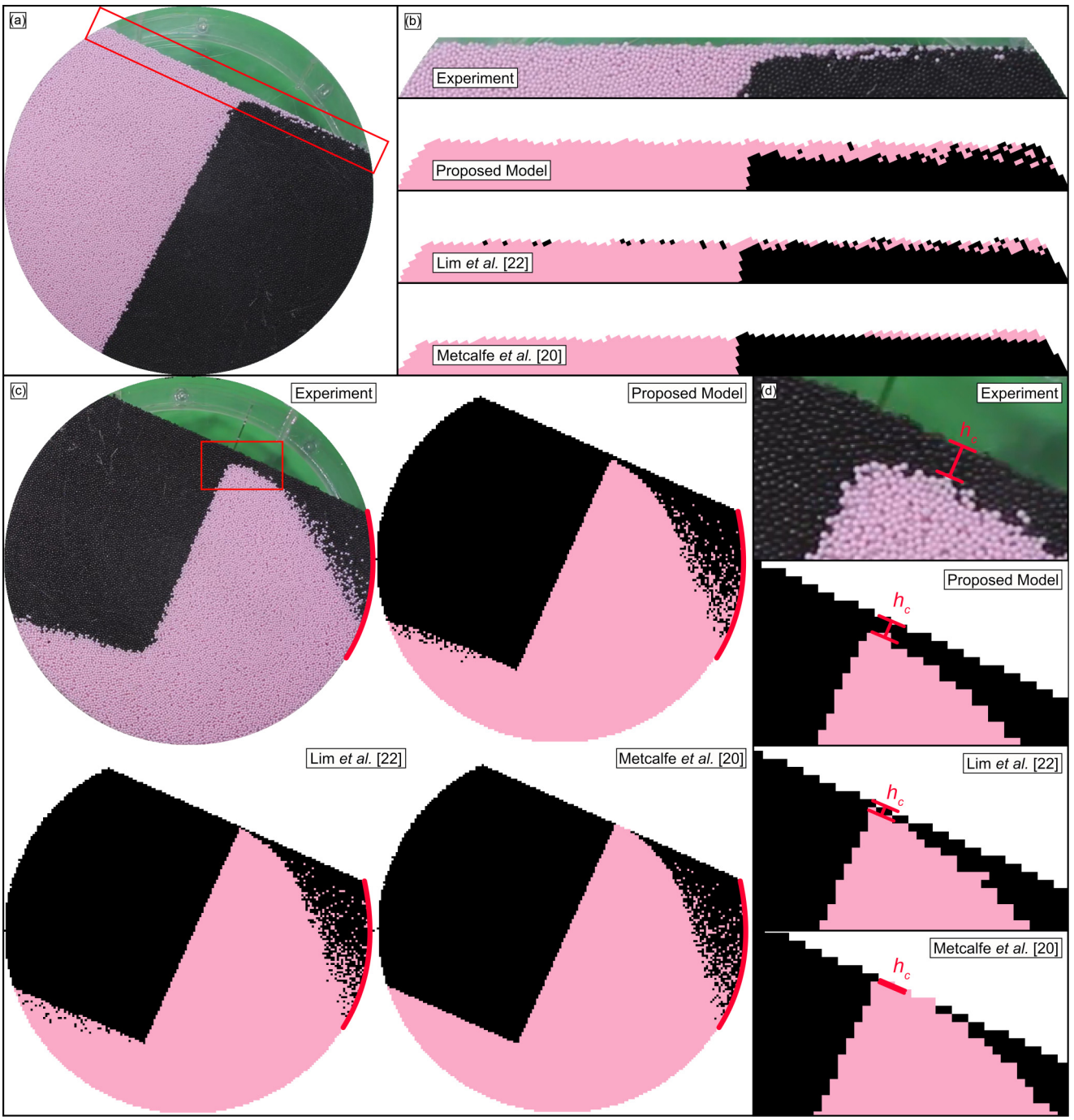

FIG. 10. Comparison between the predictions of the models of Metcalfe *et al.* [20] and Lim *et al.* [22], the newly proposed model, and experimental data. The fill level was 80% and the diameter of the cylinder was 200 mm and the length was 100 mm. The particles used in the experiments are 1–1.3 mm in diameter. The red rectangle (a) shows the area that has been zoomed into in (b). The snapshot in (a) shows the entire bed after one avalanche. The snapshots in (b) zoom into the top 20 mm of the experimental bed and plot the predictions of the models of Metcalfe *et al.* [20], Lim *et al.* [22], and the proposed model. (c) Snapshots of the beds after a rotation by 204 °. A red line spanning 59 ° is added to aid a visual comparison between the predictions of the model and the experimental data: (d) zoom into a region spanning from the top surface to the unmixed core of the bed.

in Fig. 9. Here, the flowing (avalanching) layer is split into three equal "boxes" which deform into a wedge shape over an avalanching event. In the simulation, an avalanching event occurs when the surface has reached an angle of 25 ° and after the avalanche the free surface is at an angle of 23 ° (based on the experimental results from the drum of diameter 140 mm shown in Fig. 2). The particles in the preavalanche segments "A," "B," and "C" are randomly generated (mixed) in their respective sections after the preceding avalanching event. The deformation of the initial segments during an avalanching event is shown in Fig. 9 (note the areas of each segment are preserved over an avalanche event).

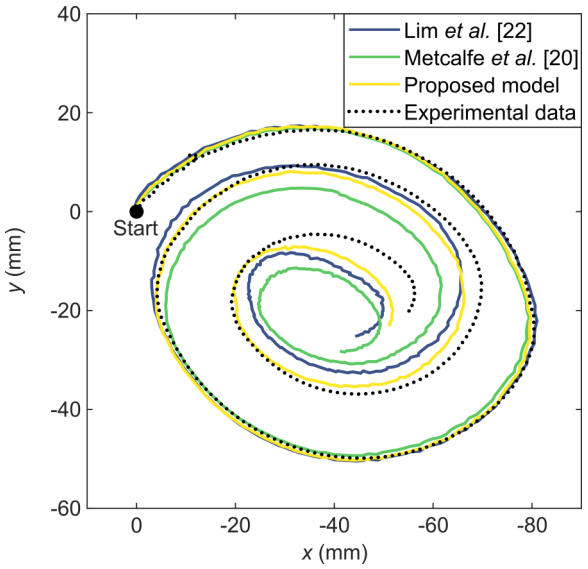

FIG. 11. Position of the center of mass of the pink particles during two drum rotations for an 80% fill level with the starting point set to (0,0). We compare our proposed model and experimental data with the models of Lim *et al.* [22] and Metcalfe *et al.* [20]. The positions are given relative to the starting point. The drum diameter was 170 mm, the fill level was 80%, the particle diameter was 1.0–1.3 mm and the drum rotated with 0.093 rpm.

This model reflects better the PIV results, i.e., particles in the middle segment travel farther than particles in the bottom segment and the same distance as particles in the top segment. Hence, although the middle section still does not move the farthest it is an improvement on both the Metcalfe *et al.* [20] and Lim *et al.* [22] models for which the top section travels the furthest down the free surface.

A schematic comparison of the distances traveled by particles located at the surface of the drum in the different models and the experiments is given in Fig. SM 4 [39]. Due to the assumption of random mixing in the simulations, particles located higher up the chord in their respective sections have a higher potential to travel further when being regenerated after the avalanching event (Fig. SM 4 [39]). Therefore, a shortcoming of our model lies in the particle dynamics in the area above the center of the chord. Yet as the particles in the top section (A) travel similar distances as the particles in the middle section, rather than larger distances as in the models of Metcalfe *et al.* [20] and Lim *et al.* [22], our model is still an improvement to the existing ones.

In order to compare the accuracy and visualize the differences between these three models, we recorded the mixing of an initially segregated bed viewed through the clear endcap of the cylinder (the pink- and black-colored particles used differ only in their color while their density and size are identical).

Visualizing the particle-mixing behavior through the end plates (see Fig. 10) is a conventional approach for evaluating the mixing of the bed [20] and, although the particle velocity is affected by the endcap walls, it provides useful information for the elaboration and validation of avalanching models.

For all models, we assumed random mixing within the segment of the free surface, although Lim *et al.* do not state explicitly this assumption (Metcalfe *et al.* [20] state explicitly that random mixing in a segment is assumed.). First, we attempted to compare the predictions of the different models with the experimental data by computing a global parameter, i.e., the center of mass of the pink particles. Figure 11 compares the position of the center of mass of the pink particles (fill level 80%, drum diameter 200 mm, particle size range 1.0–1.3 mm) predicted by the three models with the experimental measurements. The starting point is set to (0,0) and due to the direction of the x axis, the x values are negative. In the beginning, the models and the experimental data show very good agreement, while towards longer rotation times, larger differences between the individual models and the experimental data become apparent. Towards the end of the mixing experiments, it appears as if the model proposed here is closest to the experimental data, yet a clear assessment is difficult.

In a second step, we used key transition points for comparison between the models and the experimental results (Fig. 11). The first key transition point is right after the first avalanche event. A side view of the bed after the first avalanche in the simulations and experiment is provided in Figs. 10(a) and 10(b). In the experiment, we observe a pink wedge tapered to the outside of the cylinder, after the first avalanche. In the Metcalfe *et al.* [20] model, a wedge has been formed but it tapers in towards the center of the cylinder, which does not agree with the experimental observations. The wedge predicted by the model of Lim *et al.* [22] also tapers in the opposite direction (up to the highest point of the free surface) to what is observed experimentally. Owing to the particular construction of the wedges in the Lim *et al.* [22] model and with the assumption of random mixing, some black particles are predicted in the upper half of the free surface after the first avalanche. As a matter of fact, Lim *et al.* [22] do not describe how mixing occurs in the wedge and it is only mentioned that particles move on average 1/3 of the length of the chord. On the one hand, if random mixing is taking place inside the wedges and its centroid moves 1/3 of the chord length, as considered in Fig. 10, an unrealistic behavior of the black particles would take place. On the other hand, if all particles on the surface of the bed move approximately 1/3 of the chord length, the whole wedge would slide down, thus not making possible to have the wedge tapering towards the top as they predict.

The model proposed here overcomes the abovementioned limitations of both the Metcalfe *et al.* [20] and Lim *et al.* [22] models and predicts a physically realistic formation of a wedge of pink particles that is tapering in the same direction as the experiments, i.e., towards the lower edge of the free surface.

Another transition moment is when black particles start to avalanche down over the pink particles. This point in the rotation cycle allows for another comparison between the three models and experiments [Figs. 10(c) and 10(d)]. A red line along the perimeter of the cylinder of equal length allows for an easier comparison between the experiments and the different models. In the models of Lim *et al.* [22] and Metcalfe *et al.* [20], the black particles close to the perimeter have traveled farther down compared to the proposed model and the experiments. A further region that allows for a quantitative

TABLE III. Distance from the surface of the bed to the unmixed core of the bed (h_c). The unmixed core is the part of the bed that is not involved during an avalanche and which therefore remains unchanged throughout all rotations.

	h_c 60% fill (mm)	h_c 80% fill (mm)
Experiment	10.1 ± 2.0	6.6 ± 1.3
New model	4.0 ± 0.3	2.5 ± 0.5
Lim *et al.* [22]	0.9 ± 0.5	1.3 ± 0.4
Metcalfe *et al.* [20]	0.1 ± 0.2	0.2 ± 0.3

comparison is the size of the core, i.e., the unmixed center of the cylinder that exists for fill levels >50% [20]. The distance from the top of the free surface to the unmixed core, h_c, is marked in Fig. 10(d) and is used for comparison. We observe that h_c, as determined in the experiments, is larger than the value predicted in any of the models. Nonetheless, the model proposed in this work gives values of h_c that are the closest to the experimental value. Table III presents h_c for 60 and 80% fill levels, confirming quantitatively the improved accuracy of the proposed model, albeit there still exist some appreciable differences to the experimental results.

Although we have not examined the depth of the surface flow, we can compare the depth of the surface flow in our model with the experimental data of Rabaud *et al.* [36], who examined from the side walls the depth of the surface flow due to avalanches using PIV (drum diameters 170–500 mm, fill level 50%). It was found that the particle velocity decays exponentially with depth from the surface. If we consider the depth at which the particle velocity has dropped to 25% of its value at the surface as the thickness of the avalanching layer, the experiments of Rabaud *et al.* [36] yield a thickness of the flowing layer of ∼3 mm (particles of size 1.0 mm). This agrees very well with the depth of the segments used in our model, i.e., 2.9 mm.

V. CONCLUSION

PIV has been performed to examine the movement of particles along the free surface of an avalanche in a rotating cylinder. The angle of repose of the bed was also tracked.

A sawtooth pattern can be seen for the slope of the bed as a function of time. The individual avalanches can be observed by a rapid decrease in the slope angle, with each avalanche followed by a linear increase in slope angle during rigid-body rotation. As the diameter of the cylinder is increased, the avalanches become more regular, as also observed by Daerr and Douady [34].

Avalanches appear to begin from an initiation point anywhere axially on the free surface, although along the chord the initiation points are concentrated in the third quarter from the bottom. Avalanches propagate quickly such that more than 90% of the bed surface is in motion by about 20% of the duration of an average avalanche from its start. At the point when the maximum speed in an avalanche is attained, the entire bed is almost unidirectionally traveling down the chord. The particles still in motion at the end of an avalanche appear to be randomly scattered on the free surface with multidirectional velocities similar to the results of Zaitsev *et al.* [26] and Deboeuf *et al.* [38]. The distances traveled along the free surface are a function of their starting location along the chord of the free surface. The particles that travel the farthest are located at the center of the free surface. Farther from the center, the distance traveled by the particles decreased at an increasing rate. Based upon these results a revised geometric model was proposed, where the flowing surface is divided into three sections which deform into a wedge during an avalanching event. The proposed model shows a better agreement with experimental mixing data when compared to the models of Metcalfe *et al.* [20] and Lim *et al.* [22], albeit the improvement is only visible in a few specific locations.

ACKNOWLEDGMENTS

We acknowledge the Swiss National Science Foundation (Grant No. 182692) for financial support, and James Third for valuable input in the beginning of the project. This publication was created as part of NCCR Catalysis, a National Centre of Competence in Research funded by the Swiss National Science Foundation (Grant No. 180544). E.C.-P. acknowledges support from the CONEX-Plus program funded by Universidad Carlos III de Madrid and the European Union's Horizon 2020 program under the Marie Sklodowska-Curie Grant Agreement No. 801538. C.P.M. would like to thank Jens Metzger and Nicholas Conzelmann for insightful discussions.

[1] A. A. Aissa, C. Duchesne, and D. Rodrigue, Polymer powders mixing Part I: Mixing characterization in rotating cylinders, Chem. Eng. Sci. **65**, 786 (2010).

[2] F. A. O. Fontes, J. F. de Sousa, C. P. Souza, M. B. D. Bezerra, and M. Benachour, Production of Nbc from Nb2O5 in a rotating cylinder reactor: Kinetic study of reduction/carburization reactions, Chem. Eng. J. **175**, 534 (2011).

[3] D. M. Scott, J. F. Davidson, S. E. Cheah, Chua J. G. Gummow, B. P. Lam, and I. Reder, Transient granular flows in an inclined rotating cylinder: Filling and emptying, Ind. Eng. Chem. Res. **48**, 159 (2009).

[4] G. V. Prasanna Kumar, B. Srivastava, and D. S. Nagesh, Modeling and optimization of parameters of flow rate of paddy rice grains through the horizontal rotating cylindrical drum of drum seeder, Comput. Electron. Agric. **65**, 26 (2009).

[5] K. Yamane, T. Sato, T. Tanaka, and Y. Tsuji, Computer simulation of tablet motion in coating drum, Pharm. Res. **12**, 1264 (1995).

[6] G. Lu, J. R. Third, and C. R. Müller, The parameters governing the coefficient of dispersion of cubes in rotating cylinders, Granular Matter **19**, 12 (2017).

[7] G. Lu, J. R. Third, and C. R. Müller, Effect of wall roughneners on cross-sectional flow characteristics for non-spherical particles in a horizontal rotating cylinder, Particuology **12**, 44 (2014).

[8] J. R. Third, D. M. Scott, G. Lu, and C. R. Müller, Modelling axial dispersion of granular material in inclined

rotating cylinders with bulk flow, Granular Matter **17**, 33 (2015).

[9] G. Lu and C. R. Müller, Particle-shape induced radial segregation in rotating cylinders, Granular Matter **22**, 50 (2020).

[10] J. R. Third, D. M. Scott, S. A. Scott, and C. R. Müller, Tangential velocity profiles of granular material within horizontal rotating cylinders modelled using the DEM, Granular Matter **12**, 587 (2010).

[11] J. R. Third, D. M. Scott, and C. R. Müller, Axial transport within bidisperse granular media in horizontal rotating cylinders, Phys. Rev. E **84**, 041301 (2011).

[12] C. McLaren, J. R. Third, and C. R. Müller, Experimental investigation of axial dispersion in a horizontal rotating cylinder, Granular Matter **17**, 43 (2015).

[13] J. R. Third, D. M. Scott, S. A. Scott, and C. R. Müller, Effect of periodic boundary conditions on granular motion in horizontal rotating cylinders modelled using the DEM, Granular Matter **13**, 75 (2011).

[14] J. R. Third and C. R. Müller, Is axial dispersion within rotating cylinders governed by the Froude Number?, Phys. Rev. E **86**, 061314 (2012).

[15] P. Bak, C. Tang, and K. Wiesenfeld, Self-Organized Criticality: An Explanation of the $1/f$ Noise, Phys. Rev. Lett. **59**, 381 (1987).

[16] F. Cantelaube, Y. Limonuparcmeur, D. Bideau, and G. H. Ristow, Geometric analysis of avalanches in a 2D drum, J. de Phys. I **5**, 581 (1995).

[17] S. F. M. Caponeri, S. Douady, and Laroche, *Mobile Particulate Systems*, Part of the NATO ASI Series Vol. 287 (Ecole Normale Superieure de Lyon, NSSE, 1995).

[18] D. Fischer, T. Finger, F. Angenstein, and R. Stannarius, Diffusive and subdiffusive axial transport of granular material in rotating cylinders, Phys. Rev. E **80**, 061302 (2009).

[19] R. Li, H. Yang, G. Zheng, and Q. C. Sun, Granular avalanches in slumping regime in a 2D rotating drum, Powder Technol. **326**, 322 (2018).

[20] G. Metcalfe, T. Shinbrot, J. J. McCarthy, and J. M. Ottino, Avalanche mixing of granular solids, Nature (London) **374**, 39 (1995).

[21] J. J. McCarthy, T. Shinbrot, G. Metcalfe, J. E. Wolf, and J. M. Ottino, Mixing of granular materials in slowly rotated containers, AiChE J. **42**, 3351 (1996).

[22] S. Y. Lim, J. F. Davidson, R. N. Forster, D. J. Parker, D. M. Scott, and J. P. K. Seville, Avalanching of granular material in a horizontal slowly rotating cylinder: PEPT studies, Powder Technol. **138**, 25 (2003).

[23] S. Courrech du Pont, R. Fischer, P. Gondret, B. Perrin, and M. Rabaud, Instantaneous Velocity Profiles during Granular Avalanches, Phys. Rev. Lett. **94**, 048003 (2005).

[24] S. Kiesgen de Richter, V. Y. Zaitsev, P. Richard, R. Delannay, G. L. Caër, and V. Tournat, Experimental evidence of ageing and slow restoration of the weak-contact configuration in tilted 3D granular packings, J. Stat. Mech. (2010) P11023.

[25] N. Gravish and D. I. Goldman, Effect of volume fraction on granular avalanche dynamics, Phys. Rev. E **90**, 032202 (2014).

[26] V. Y. Zaitsev, P. Richard, R. Delannay, V. Tournat, and V. E. Gusev, Pre-avalanche structural rearrangements in the bulk of granular medium: Experimental evidence, Europhys. Lett. **83**, 64003 (2008).

[27] V. Salinas, C. Quiñinao, S. González, and G. Castillo, Triggering avalanches by transverse perturbations in a rotating drum, Sci. Rep. **11**, 1 (2021).

[28] Z. Wang and J. Zhang, Fluctuations of particle motion in granular avalanches - from the microscopic to the macroscopic scales, Soft Matter **11**, 5408 (2015).

[29] R. Y. Yang, A. B. Yu, L. McElroy, and J. Bao, Numerical Simulation of Particle Dynamics in Different Flow Regimes in a Rotating Drum, Powder Technol. **188**, 170 (2008).

[30] L. E. Silbert, D. Ertaş, G. S. Grest, T. C. Halsey, D. Levine, and S. J. Plimpton, Granular flow down an inclined plane: Bagnold scaling and rheology, Phys. Rev. E **64**, 051302 (2001).

[31] Q. J. Zheng and A. B. Yu, Modelling the granular flow in a rotating drum by the Eulerian finite element method, Powder Technol. **286**, 361 (2015).

[32] J. K. Sveen, An introduction to matpiv v. 1.6. 1. Eprint no. 2, Dept. of Mathematics, University of Oslo (2004).

[33] R. D. Keane and R. J. Adrian, Theory of cross-correlation analysis of PIV images, Appl. Sci. Res. **49**, 191 (1992).

[34] A. Daerr and S. Douady, Two types of avalanche behaviour in granular media, Nature (London) **399**, 241 (1999).

[35] N. A. Pohlman, S. W. Meier, R. M. Lueptow, and J. M. Ottino, Surface velocity in three-dimensional granular tumblers, J. Fluid Mech. **560**, 355 (2006).

[36] M. Rabaud, R. Fischer, S. Courrech du Pont, P. Gondret, and B. Perrin, Dynamique Des Avalanches Granulaires, 17ème Congrès Français de Mécanique (2005).

[37] N. J. Balmforth and J. N. McElwaine, From episodic avalanching to continuous flow in a granular drum, Granular Matter **20**, 52 (2018).

[38] S. Deboeuf, E. M. Bertin, E. Lajeunesse, and O. Dauchot, Jamming transition of a granular pile below the angle of repose, Eur. Phys. J. B **36**, 105 (2003).

[39] See Supplemental Material at http://link.aps.org/supplemental/10.1103/PhysRevE.106.054902 for details on the distance traveled during an avalanche as a function of particle diameter and fill height and different geometric models.